JOURNAL OF SPACECRAFT AND ROCKETS
Vol. 38, No. 3, May–June 2001

Three-Dimensional Particle Simulations of Ion Propulsion Plasma Environment for Deep Space 1

J. Wang* and D. Brinza†
Jet Propulsion Laboratory, California Institute of Technology, Pasadena, California 91109
and
M. Young‡
University of Southern California, Los Angeles, California 90089

A fully three-dimensional particle-in-cell simulation model was developed to compute the ion propulsion induced plasma environment for the Deep Space 1 (DS1) spacecraft. Simulations are compared with in-flight measurements of charge-exchange plasma from the ion propulsion diagnostics subsystem on DS1, and the results show good agreement. It is found that the plasma environment of DS1 is dominated by the charge-exchange plasma from the plume. For a typical ion thruster operating condition, the charge exchange plasma near the spacecraft surface has a density ranging from 10^6 cm^{-3} near the thruster to 10^4 cm^{-3} at the opposite end of the spacecraft and a current density ranging from 10^{-7} A/cm^2 to 10^{-9} A/cm^2. It is shown that, for an interplanetary spacecraft with a moderate charging potential, charge-exchange ion backflow is through an expansion process similar to that of the expansion of a mesothermal plasma into a vacuum.

Nomenclature

A_n	=	ion optics flow-through area
$\boldsymbol{E}$	=	electric field
E_b	=	beam ion energy
I_b	=	beam ion current
J_{b0}	=	average beam ion current density at the thruster exit
J_{cex}	=	charge-exchange ion current density
m_{Xe}	=	xenon atom mass
$\dot{N}_n$	=	neutral Xe particle flux
n_b, n_n, n_{cex}	=	number density for the beam ions, the neutrals, and the charge-exchange ions, respectively
n_{b0}, n_{n0}, n_{cex0}	=	average number density at the thruster exit for the beam ions, the neutrals, and the charge-exchange ions, respectively
n_e, n_i	=	electron and total ion (beam ion plus charge exchange ion) number density, respectively
T_e	=	electron temperature
T_w	=	thruster wall temperature
v_b, v_{cex}	=	beam ion drift velocity and charge-exchange ion velocity, respectively
η_d	=	discharge propellant efficiency
λ_D^{cex}	=	debye length in the charge-exchange plasma
σ_{cex}	=	charge-exchange collision cross section
Φ	=	electric potential
Φ_{IDS}, Φ_{p0}	=	local plasma potential at the ion propulsion diagnostic system (IDS) location and the thruster exit, respectively
Φ_p	=	plasma potential within the ion beam
Φ_{sc}, Φ_{scg}	=	potential of the spacecraft and spacecraft ground, respectively

Received 9 June 2000; revision received 1 December 2000; accepted for publication 20 December 2000. Copyright © 2001 by the American Institute of Aeronautics and Astronautics, Inc. The U.S. Government has a royalty-free license to exercise all rights under the copyright claimed herein for Governmental purposes. All other rights are reserved by the copyright owner.

*Principal Member of Engineering Staff; currently Associate Professor, Department of Aerospace and Ocean Engineering, Virginia Polytechnic Institute and State University, Blacksburg, VA 24061-0203. Member AIAA.
†Senior Systems Engineer, MS 125-177.
‡Graduate Research Assistant, Department of Aerospace and Mechanical Engineering. Student Member AIAA.

I. Introduction

ION propulsion devices are valued as a high-specific impulse class of space propulsion. NASA's New Millennium Deep Space One (DS1) marks the beginning of interplanetary missions using spacecraft operated with ion propulsion. Using a 30-cm-diam Xe ion thruster as its primary propulsion, DS1 successfully flew by asteroid Braille on 28 July 1999 and is currently on a trajectory for a possible encounter with comet Borrelly in 2001.

An ion thruster propels a spacecraft by continuously emitting a partially ionized gas. An ion thruster plume is composed of propellant efflux (high-energy beam ions, neutralizing electrons, and un-ionized neutrals that escaped through the ion optics and from the neutralizer), nonpropellant efflux (material sputtered from thruster components and the neutralizer), and a low-energy charge-exchange plasma generated by collisions between the beam ions and the neutrals within the plume. It is well known that both the low-energy charge-exchange ions and the ionized sputtered particles can be pushed out of the plume by the local electric field and backflow to interact with the spacecraft.[1,2]

The propellant charge-exchange ion is the dominant backflow species. The characteristics of ion thruster plume–spacecraft interactions are primarily determined by the charge-exchange plasma environment. Charge-exchange ions can affect spacecraft charging by interacting with the solar arrays and any exposed conducting surface. These ions can also affect space plasma measurements performed onboard by interacting with the ambient plasma and by dominating the local plasma environment surrounding the spacecraft. The Xe charge-exchange ions do not directly contaminate spacecraft surfaces because Xe is not a contaminating species. Spacecraft contamination is caused by the backflow of sputtered grid material, which, in the case of DS1, is molybdenum. Deposition of molybdenum particles on the spacecraft surface can significantly change the thermo-optical (solar absorptance and emittance) properties of thermal control materials. However, the charge-exchange plasma may play an important role in the backflow of contaminating species through its effects on the electric field and plasma sheath surrounding the spacecraft, which in turn controls the trajectories of any ionized particles near the spacecraft. Effects from charge-exchange plasma interactions are especially important for interplanetary spacecraft. The density of the solar wind plasma is only about 1–10 particles per centimeter cubed, and, thus, the spacecraft plasma environment will be dominated by the charge-exchange plasma from the thruster plume.

The DS1 mission provides the first comprehensive in-flight investigation of ion thruster plume–spacecraft interactions. DS1 carries an integrated set of ion propulsion diagnostics, ion propulsion

diagnostic system (IDS), and a state-of-the-art plasma sensor, the plasma experiment for planetary exploration (PEPE). Both IDS and PEPE have produced high-quality data concerning ion thruster plume–spacecraft interactions. DS1 measurements of the ion propulsion plasma environment were recently reported by Wang et al.[3] DS1 measurements of ion propulsion contamination are reported by Brinza et al.[4] Because IDS and PEPE make only single point measurements, modeling is essential to provide a more complete description of plume–spacecraft interactions. A set of computer particle simulation-based numerical models has been developed to assist the data analysis and interpretation. This paper reports results from a modeling investigation of the ion propulsion plasma environment of DS1.

Computer particle simulation has proven to be the best tool available for modeling plasma plume–spacecraft interactions. Recently, several computer particle simulation models have been developed for ion thruster plumes.[5–8] However, most of the simulation studies published so far have focused on the region downstream of the thruster exit. None of the published studies have modeled the charge-exchange plasma in the entire upstream region of the thruster exit. It is the upstream region that is most relevant for assessment of effects from plume–spacecraft interactions.

In this paper, we present a three-dimensional particle-in-cell model that simulates charge-exchange ion interactions over the entire downstream-to-upstream region surrounding a spacecraft with an ion thruster. With measured in-flight ion thruster operation parameters used as input, this model is applied to obtain the ion propulsion induced plasma environment surrounding DS1. Section II briefly describes the DS1 spacecraft, ion thruster operation parameters, and in-flight measurements of the ion propulsion charge-exchange plasma. Section III discusses the simulation model. Section IV presents simulation results and compares them with in-flight measurements. Section V contains conclusions.

II. DS1 Spacecraft and In-Flight Measurement

A. Spacecraft

Figure 1 illustrates the DS1 spacecraft with deployed solar arrays. The DS1 spacecraft bus plus the propulsion module is essentially a hexagon cylinder of about 1.6 m in height and 1.2 m in diameter. In the local coordinate system shown in Fig. 1, the spacecraft orientation is such that the thrust vector is along the $-z$ axis and the solar array face is almost always facing the $+x$ axis.

The solar concentrator arrays with refractive linear element technology (SCARLET) solar array has a voltage span of 100 V. The solar array support panel is made of graphite/epoxy face sheets on aluminum honeycomb. The concentrator connectors are covered by insulating materials to prevent arcing. Both the spacecraft and the solar array support panel are grounded at the 0-V end of the SCARLET solar array.

A close-up view of the DS1 spacecraft with the PEPE and IDS instruments is illustrated in Fig. 1 of Ref. 4. The plasma sensors of IDS include a retarding potential analyzer (IDS-RPA) and a planar Langmuir probe (IDS-LP1). IDS-RPA and IDS-LP1 are collocated at about 75 cm from the thruster centerline. PEPE is located on the surface at the opposite end from the thruster. For detailed discussions of the IDS and PEPE instruments, the reader is referred to Refs. 3 and 4.

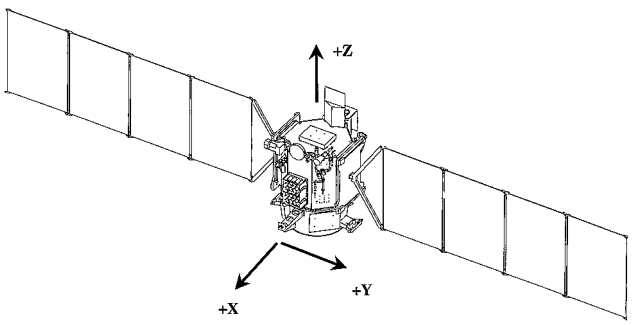

Fig. 1 DS1 spacecraft.

B. Ion Thruster Plume

The 30-cm-diam NASA solar electric propulsion technology application readiness (NSTAR) Xe ion thruster used on DS1 has an input power range of 500–2300 W. The propellant Xe ions are accelerated through a Mo grid to form a beam with an energy E_b up to 1100 eV (exit beam velocity of $v_b \simeq 3.5 \times 10^6$ cm/s) and a current I_b up to 1.8 A. At full thrust level, the thruster produces a thrust of 92 mN and a specific impulse of about 3100 s. Measurements have shown that the propellant ions form a divergent beam with a divergence half angle of about 15–20 deg due to the curvature of the thruster exit surface. The ion beam is kept quasi neutral by electrons emitted from the neutralizer.

The propellant that remains un-ionized flows out of the thruster exit in free molecular flow with a thermal speed corresponding to the thruster wall temperature of $T_w \sim 500$ K (0.04 eV). The density of the neutral plume typically remains quasi steady due to the low charge-exchange collision rate. One can estimate the average neutral density at thruster exit n_{n0} from the measured main flow rate, cathode flow rate, and the discharge propellant efficiency η_d. If the un-ionized propellant exits through the grids in free-molecular flow with a temperature close to that of the thruster discharge chamber walls T_w, n_{n0} can be calculated from

$$n_{n0} = \dot{N}_n \Big/ \left(A_n \sqrt{8kT_w/\pi m_{\mathrm{Xe}}}\right) \tag{1}$$

where $\dot{N}_n$ is the number of Xe atoms flowing out of the thruster per second and is obtained from the discharge chamber flow rate.[3] A_n is the flow-through area through the grids and is about 0.24 of the thruster exit area for the NSTAR thruster.

Charge-exchange collisions occur between the beam ions and the neutrals. The average charge exchange ion production rate at the thruster exit is given by

$$\frac{\mathrm{d}n_{\mathrm{cex0}}}{\mathrm{d}t} = n_{b0} n_{n0} v_b \sigma_{\mathrm{cex}} \tag{2}$$

where n_{b0} is the average beam ion density at the thruster exit $[n_{b0} = I_b/(ev_bA)]$ and σ_{cex} the charge-exchange ion collision cross section; σ_{cex} can be estimated from curve fitting of the measured collision cross section for $Xe^+ - Xe$ charge-exchange[5,9]:

$$\sigma_{\mathrm{cex}} = (k_1 \ln v_b + k_2)^2 \times 10^{-16} \text{ cm}^2 \tag{3}$$

where v_b is beam ion velocity in meters per second, $k_1 = -0.8821$, and $k_2 = 15.1262$.

C. Engine Parameter and In-Flight Measurement

The NSTAR ion thruster can be operated over a wide range of engine parameters.[10] A thruster flight throttle table is also listed in Table 1 of Ref. 4. For comparison with in-flight measurement, we consider a typical engine operating condition in this paper, mission throttle level (ML) 83. ML 83 is chosen because it is one of the highest power levels at which the thruster has operated during the entire DS1 mission. It is also an operating condition that was monitored by simultaneous IDS and PEPE measurements.[3] ML 83 has an engine input power of 1.82 kW and a specific impulse of 3189 s. From flight data, we find the values of beam current I_b, beam ion energy E_b, and discharge propellant efficiency η_d for ML 83 to be $I_b \simeq 1.40$ A, $E_b \simeq 1095$ eV, and $\eta_d \simeq 0.88$, respectively.[3] Using these data, one readily calculates the beam plasma density, neutral density, and the charge-exchange ion production rate near the thruster exit. The results are listed in Table 1.

Table 1 Thruster operating condition from in-flight engine data

Parameter	Value
Thrust level	ML 83
J_{b0}, A/m^2	19.8
V_{b0}, km/s	38.7
n_{b0}, 1/cm^3	3.22×10^9
$\dot{N}_{n0}$, 1/s	1.1×10^{18}
n_{n0}, 1/cm^3	0.23×10^{12}
$\mathrm{d}n_{\mathrm{cex0}}/\mathrm{d}t$, 1/cm^{3}s	1.0×10^{13}

Table 2 Charge-exchange plasma environment for ML83 at IDS: in-flight measurement and simulation result

Measurement	$\Phi_p - \Phi_{scg}$, V	T_e, eV	J_{cex}, A/cm^2	n_{cex}, cm^{-3}
IDS data	19	2.09	0.9×10^{-7} to 3.3×10^{-7}	1.2×10^6 to 4.4×10^6
Simulation	Input	Input	1.49×10^{-7}	1.43×10^6

The induced plasma environment for ion thruster operation at ML 83 was measured by both IDS and PEPE on 22 January 1999.[3] From IDS measurements, we have obtained the average plume potential Φ_p with respect to the potential of the spacecraft ground Φ_{scg} and the local plasma conditions at the location of IDS, including the plasma potential Φ_{IDS} with respect to Φ_{scg}, the charge-exchange ion current density J_{cex} and number density n_{cex}, and electron temperature T_e. The results are listed in the upper part of Table 2 and will be discussed in Sec. IV. PEPE also observed the Xe charge-exchange ions and has conclusively shown that charge-exchange ions from the plume can backflow to the opposite side of the spacecraft. PEPE data are still being analyzed to obtain physical parameters for the charge-exchange plasma.

PEPE has a lower energy cutoff of ± 8 V for instrument protection. The DS1 spacecraft floating potential cannot be determined from PEPE measurements of the solar wind because it falls under this lower energy threshold. PEPE measurements during the mission have suggested that any change in spacecraft potential due to ion thruster operation is within the ± 8-V range.

III. Three-Dimensional Particle Simulation Model

A three-dimensional electrostatic particle-in-cell (PIC) code is developed to solve self-consistently the particle trajectories and space charge for the charge-exchange plasma and the electric field surrounding the spacecraft. Because our emphasis here is on charge exchange ion backflow, only the charge-exchange ions are treated as test particles.

The basic formulation for charge-exchange ion production is similar to that used in Ref. 5. The density distribution of the propellant beam ions $n_b(\boldsymbol{x})$ is modeled by an analytical profile because the propellant beam ions follow a ballistic trajectory due to their high energy. We assume that the radial current density profile of the beam ions consists of a parabolic core and an exponential wing. The density distribution of the neutral plume $n_n(\boldsymbol{x})$ is also modeled analytically as that of a free molecular flow from a point source located at one thruster radius r_T behind the thruster exit. The density distribution of the neutral plume is given by[5]

$$n_n(R,\theta) = a n_{n0}\left\{1 - \left[1 + (r_T/R)^2\right]^{-\frac{1}{2}}\right\}\cos\theta \tag{4}$$

where R is the distance to the point source, θ is the angle between R and the downstream axis, and a is a correction factor. Using the analytical profiles for the beam ions and the neutral plume, one obtains the spatial distribution of the charge-exchange ion production rates

$$\frac{\mathrm{d}n_{cex}}{\mathrm{d}t} = n_b(\boldsymbol{x}) n_n(\boldsymbol{x}) v_b \sigma_{cex} = \frac{n_b(\boldsymbol{x})}{n_{b0}} \frac{n_n(\boldsymbol{x})}{n_{n0}} \left(\frac{\mathrm{d}n_{cex0}}{\mathrm{d}t}\right) \tag{5}$$

where $\mathrm{d}n_{cex0}/\mathrm{d}t$ is the average charge exchange ion production rate at the thruster exit. The values n_{b0}, n_{n0}, and $\mathrm{d}n_{cex0}/\mathrm{d}t$ can be obtained from ion engine operation parameters, as discussed.

Boyd et al.[11] recently used the direct simulation Monte Carlo (DSMC) method to compute the neutral plume for the UK-10 ion thruster and examined the accuracy of the analytical neutral plume model of Eq. (4). They found reasonable agreement between Eq. (4) and the DSMC result in the near-axis region but noted substantial errors in Eq. (4) in the off-axis region. Here, Eq. (4) is only used to calculate the charge-exchange ion production rate in Eq. (5). Because the beam ion density n_b concentrates along the plume axis, charge-exchange collisions occur primarily in the near-axis region (see results in the next section). Hence, the errors in Eq. (4) in the off-axis region has little effect on our results.

Test particles representing charge-exchange ions are generated at each time step according to the volumetric production rate of Eq. (5). These macroparticles are assumed to follow initially a Maxwellian velocity distribution with a temperature corresponding to that of the un-ionized neutral propellant (0.04 eV). Because the initial energy of the charge-exchange ions is negligible compared to the plume potential, the initial velocity distribution plays no role in the final results. The trajectory of each charged particle is integrated from

$$m\frac{\mathrm{d}\boldsymbol{v}}{\mathrm{d}t} = \boldsymbol{F} = q\left(\boldsymbol{E} + \boldsymbol{v} \times \frac{\boldsymbol{B}}{c}\right), \qquad \frac{\mathrm{d}\boldsymbol{x}}{\mathrm{d}t} = \boldsymbol{v} \tag{6}$$

using a standard leapfrog scheme.[12] A gather step interpolates the fields from grid points to particle positions, and a scatter step deposits the charge of each test particle to grid points.[12]

A common assumption in plasma plume modeling is that the electrons are isothermal and the electron density may be described by the Boltzmann relationship.[5–8] In principle, one may employ full particle simulations using test particles to represent both the ions and electrons. Such an approach has been applied recently for a field-emitter electric propulsion thruster plume.[13] Full particle simulations typically require the use of an artificial ion to electron mass ratio to reduce the difference between the electron and ion timescales for computational reasons. The plasma plume is a mesothermal plasma, that is, the directed ion velocity is much larger than the ion thermal velocity but much smaller than the electron thermal velocity. To model correctly a mesothermal plasma in a full particle simulation model, an extremely large ion to electron mass would need to be used. This makes the full particle approach computationally very ineffective and expansive for our problem. Hence, the assumption of a Boltzmann electron distribution is also adopted in this study.

We take the reference point for the electron density distribution to be at the thruster exit, and the electron density is given by

$$n_e = n_{e0} \exp[(\Phi - \Phi_{p0})/T_e] \tag{7}$$

where $n_{e0} = n_{b0}$ is the average plasma density at thruster exit and Φ_{p0} is the plume potential near the thruster exit. The electron temperature is a constant. In previous studies, such as Ref. 5, the reference point is taken to be the ambient plasma condition, implying that the neutralization of charge-exchange ions is provided by the ambient electrons. Such an assumption is not appropriate here because the DS1 ion thruster operates in the interplanetary plasma environment where the median observed solar wind density is $n_{sw} \simeq 6.9$ cm^{-3} (Ref. 14). At such a low density, the ambient plays no role in neutralizing the charge-exchange ions. The nature of this model is such that both the electron temperature T_e and the plume potential Φ_{p0} need to be specified by other means. In our simulations, the values for T_e and the plume potential with respect to spacecraft, $\Phi_{p0} - \Phi_{sc}$, are taken from in-flight IDS measurements.

The self-consistent electric field and space charge are obtained from Poisson's equation

$$\nabla^2 \Phi = -4\pi e\{n_i - n_{e0} \exp[(\Phi - \Phi_{p0})/T_e]\} \tag{8}$$

where n_i is the total ion charge density. To solve this nonlinear Poisson's equation in a three-dimensional space, we have employed a dynamic alternating direction implicit (DADI) method[15,16] with a defect correction using the Douglass–Gunn operator splitting[17] (see also Ref. 18). This DADI method was chosen over other algorithms for its increased stability properties over fully explicit methods and its relatively simple tridiagonal system of equations produced by the partially implicit nature of the method. The alternating direction implicit (ADI) method first introduces a fictitious time derivative. An initial guess, typically the potential at the previous real-time level, is then advanced until steady-state conditions are reached. At the steady-state condition, the time derivative vanishes, leaving the original equation. The ADI method splits the spatial operator

along the coordinate directions. Each time step is, therefore, split into a sequence of substeps, each with only one operator acting implicitly. The defect correction implementation of the Douglass–Gunn operator splitting[17] is given by

$$\left(-\frac{1}{\Delta t}+\frac{H}{2}\right)d' = \mathrm{Res}(S^n), \qquad \left(-\frac{1}{\Delta t}+\frac{V}{2}\right)d'' = -\frac{1}{\Delta t}d'$$

$$\left(-\frac{1}{\Delta t}+\frac{N}{2}\right)d^* = -\frac{1}{\Delta t}d'' \tag{9}$$

where H, V, and N are the spatial operators for each coordinate direction, Res is the residual operator, and d is the defect. The spatial operators are generated through second-order central differencing. The solution at the new time step is given by

$$S^{n+1} = S^n + d^* \tag{10}$$

The nonlinear source term is updated after each application of the (H, V, N) set of operators. DADI automatically adjusts the fictitious time step by comparing two separate solutions to the problem. The first solution, $\bar{S}^{n+1}$, is obtained from a single application of the (H, V, N) set of operators. The second, typically more accurate solution, S^{n+1}, is obtained from completing two sequential applications of the (H, V, N) set of operators, each with half of the fictitious time step. A test parameter is then used to estimate the amount of error associated with taking the larger time step to calculate the acceleration factor for the next ficticious time step:

$$TP = \frac{||S^{n+1} - \bar{S}^{n+1}||}{||S^{n+1} - S^n||} \tag{11}$$

Each spatial grid point, including the boundaries, can be defined as open or solid point, allowing for physical objects inside the computational domain and grid-point specific Neumann or Dirichlet conditions on the boundary.

The simulation setup is shown in Fig. 2. We model the DS1 spacecraft as a hexagonal cylinder and the solar array as a thin plate. The cylinder and the backside of the solar array are conductors with a uniform spacecraft potential Φ_{sc}. The front face of the solar array is covered by glass and, thus, is an insulator. It typically has a surface voltage of about $-T_e$, where T_e is the temperature of the electrons surrounding the solar array in electron volts. This solar array model is sufficient for our purpose because all of the high-voltage connectors on the solar array are covered by insulating materials. Moreover, any potential leakage from the edge of the solar array will

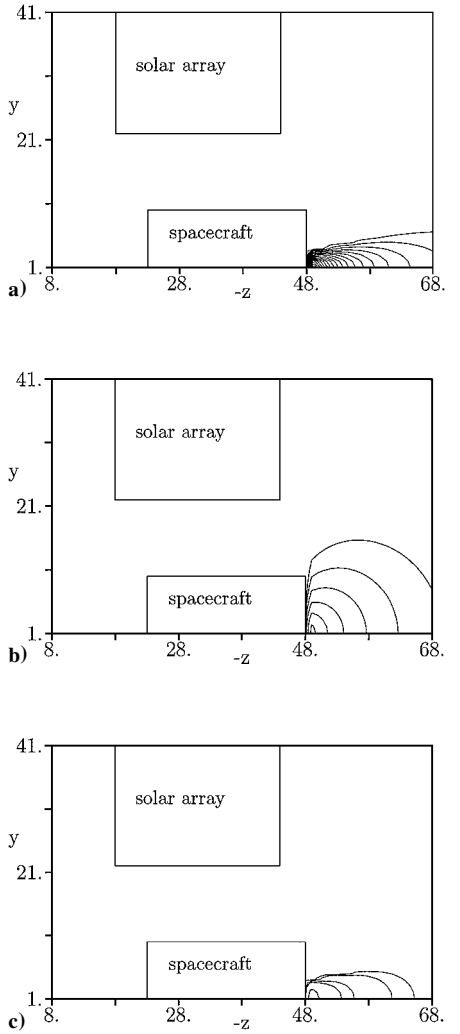

Fig. 3 Beam ion density, neutral plume density, and charge-exchange ion production rate on a *zy* plane cutting through the thruster center at $-x = 1$: a) beam ion number density (contour levels from outside toward the thruster exit: n_b/n_{b0} from 0.05 to 1 with an interval of 0.05), b) neutral plume density (contour levels from outside toward the thruster exit: n_n/n_{n0} = 0.025, 0.05, 0.1, 0.2, 0.4, and 0.8), and c) charge-exchange ion production rate (contour levels from outside toward the thruster exit: $(dn_{cex}/dt)/(dn_{cex0}/dt)$ = 0.005, 0.01, 0.05, 1., 0.5, and 1).

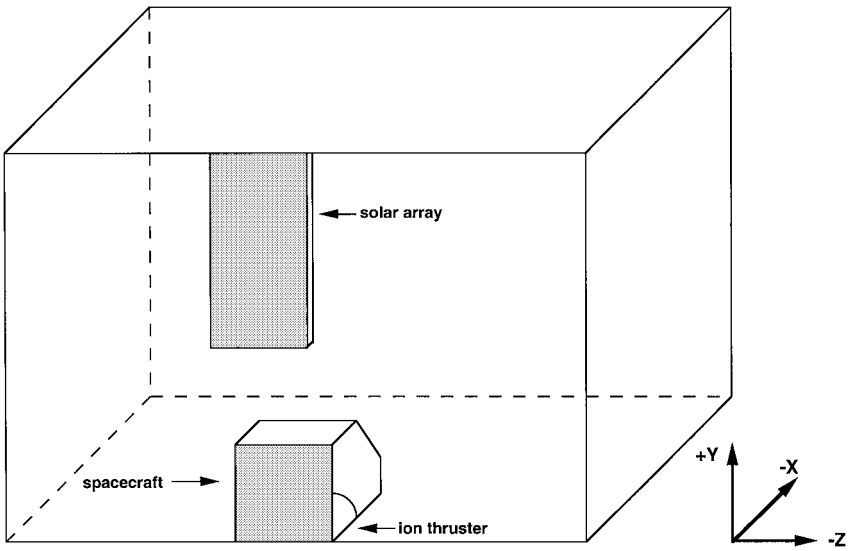

Fig. 2 Simulation model.

be shielded out within a few debye lengths by the charge-exchange plasma.

When geometric symmetry is accounted for, the simulation setup needs to include only a quarter of the spacecraft and part of one solar array. We take the simulation domain to be in the $-x$, y, and $-z$ region. The origin of the coordinate system is at $(-x, y, -z) = (1, 1, 1)$. The spacecraft centerline is placed at the $(-x, y) = (1, 1)$ axis, and the thrust vector is along the $-z$ direction. The solar array panel lies on the $-x = 1$ boundary. Its surface facing into the simulation domain is the backside of the solar array (which has a surface potential of Φ_{sc}). The conditions at $-x = 1$ and $y = 1$ boundaries are that for a symmetric face. All other boundaries are considered open boundaries. Because computationally it is not feasible to set the simulation domain large enough for the outer boundary to be the undisturbed ambient plasma, a Neumann condition $\nabla \Phi_n = 0$ is used at all open boundaries.

Out of consideration for computational efficiency and speed for large-scale three-dimensional simulations, the computational grid is chosen to consist of uniform cells. To capture the details in the high-density region near thruster exit, one could use an adaptive grid such as tetrahedral cells or nonorthogonal grids. However, these PIC codes are significantly more computationally expensive than a standard orthogonal grid PIC code because of the added complexity and memory references needed for particle tracking.[18] Our main interest is in the region outside of the ion beam where the charge-exchange plasma density is significantly lower than that at the thruster exit.

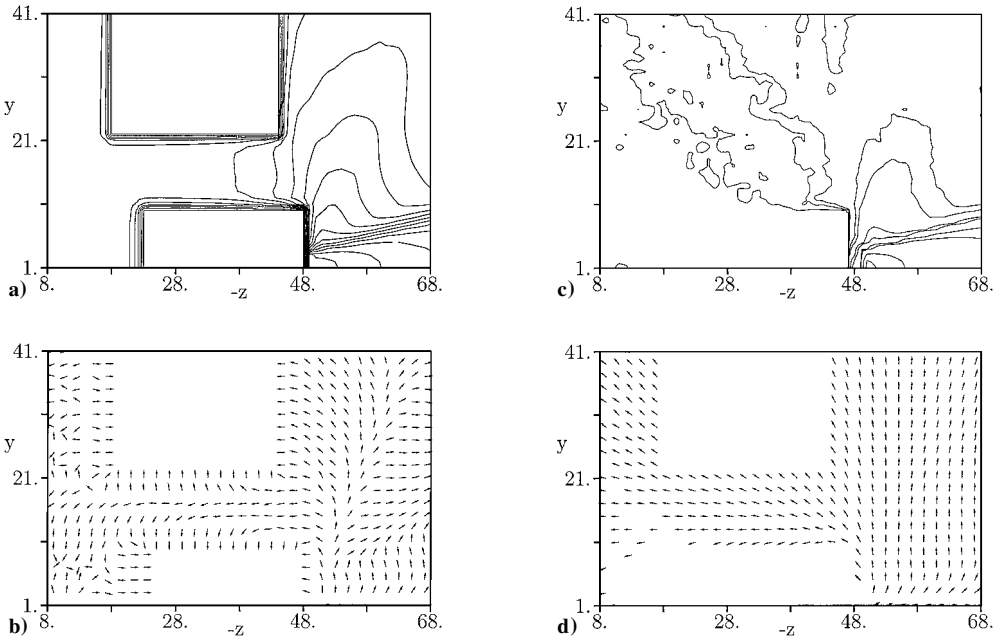

Fig. 4 Simulation results on a zy plane at $-x = 1$: a) electric potential (contour levels clockwise from the spacecraft and the solar array toward the thruster exit: $\Phi - \Phi_{sc}$ from 0 to 19 V with an interval of 1 V), b) vector plots for electric field $E/|E|$, c) total ion number density (contour levels clockwise from the spacecraft surface toward the thruster exit: $n_i = 10^4, 5 \times 10^4, 10^5, 5 \times 10^5, 10^6, 5 \times 10^6, 10^7, 5 \times 10^7, 10^8, 5 \times 10^8$, and 10^9 particles/cm^3), and d) vector plots for charge-exchange ion velocity $J_{cex}/|J_{cex}|$.

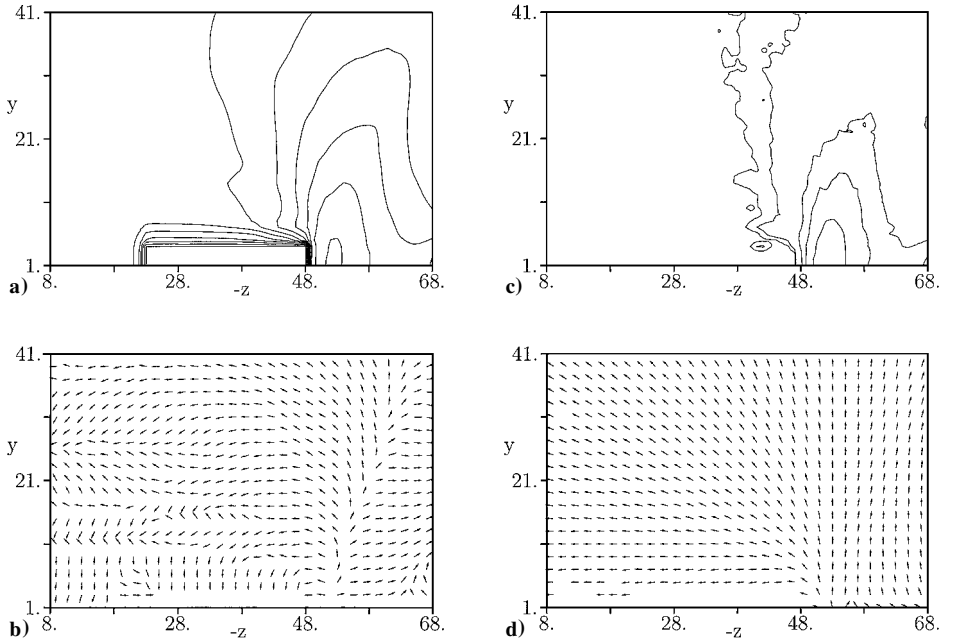

Fig. 5 Simulation results on a zy plane at $-x = 10$: a) electric potential (contour levels clockwise from the spacecraft surface to the z axis: $\Phi - \Phi_{sc}$ from 0 to 19 V with an interval of 1 V), b) vector plots for electric field $E/|E|$, c) total ion number density (contour levels clockwise from the spacecraft surface to the z axis: $n_i = 10^4, 5 \times 10^4, 10^5, 5 \times 10^5, 10^6$, and 2×10^6 particles/cm^3), and d) vector plots for charge-exchange ion velocity $J_{cex}/|J_{cex}|$.

Hence, we find that it is much more efficient to apply the computational resources on tracking more particles to increase the particle statistics in the backflow region.

In the simulations, the grid resolution is determined by the debye length of the charge exchange plasma in the region outside of the ion beam, λ_D^{cex}. We choose the grid size to be of the same order of magnitude of the local λ_D^{cex} in the region surrounding the ion beam near the thruster exit. Note that such a grid size is always smaller than the local λ_D^{cex} in the backflow region. Typically, the local charge exchange plasma density is not known a priori, and the grid resolution needs to be determined through trial and error. However, in this study, IDS measurements provide a convenient guideline for setting the grid resolution. A series of simulations using various grid sizes were performed to ensure that the results are not affected by the chosen grid resolution.

IV. Results and Discussion

In this section, we present simulation results for the ion engine operating condition ML 83. As discussed in last section, the input parameters for the simulation model are n_{b0}, n_{n0}, dn_{cex0}/dt, T_e, and $\Phi_{p0} - \Phi_{sc}$. The values for n_{b0}, n_{n0}, and dn_{cex0}/dt are obtained from ion engine operation parameters, and are listed in Table 1. IDS measured T_e and the average plume potential near the thruster exit Φ_p with respect to the spacecraft ground Φ_{scg}. To a good approximation, we assume $\Phi_{p0} - \Phi_{sc} \simeq \Phi_p - \Phi_{scg}$. The measured values for T_e and $\Phi_p - \Phi_{scg}$ are listed in Table 2.

In the simulation, the potential on the spacecraft and solar array surface is set at Φ_{sc}. We emphasize that the electric potential of the spacecraft–plume system is floating with respect to the ambient plasma. Hence, only the relative potential difference is a meaningful parameter. The relative potential difference between Φ_{sc} and the

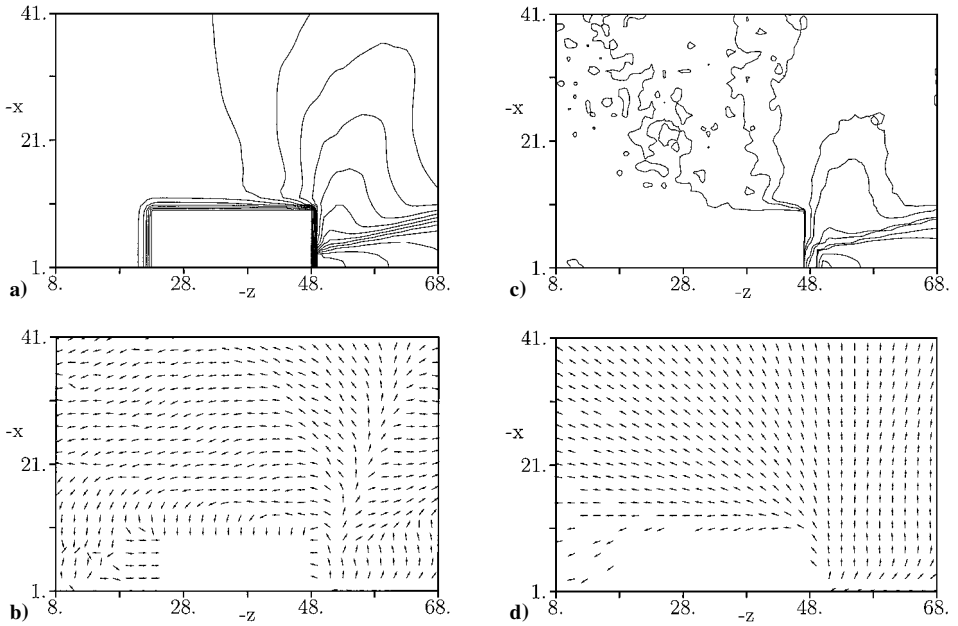

Fig. 6 Simulation results on a zx plane at $y = 1$: a) electric potential (contour levels clockwise from the spacecraft surface toward the thruster exit: $\Phi - \Phi_{sc}$ from 0 to 19 V with an interval of 1 V), b) vector plots for electric field $E/|E|$, c) total ion number density (contour levels same as that in Fig. 4), and d) vector plots for charge-exchange ion velocity $J_{cex}/|J_{cex}|$.

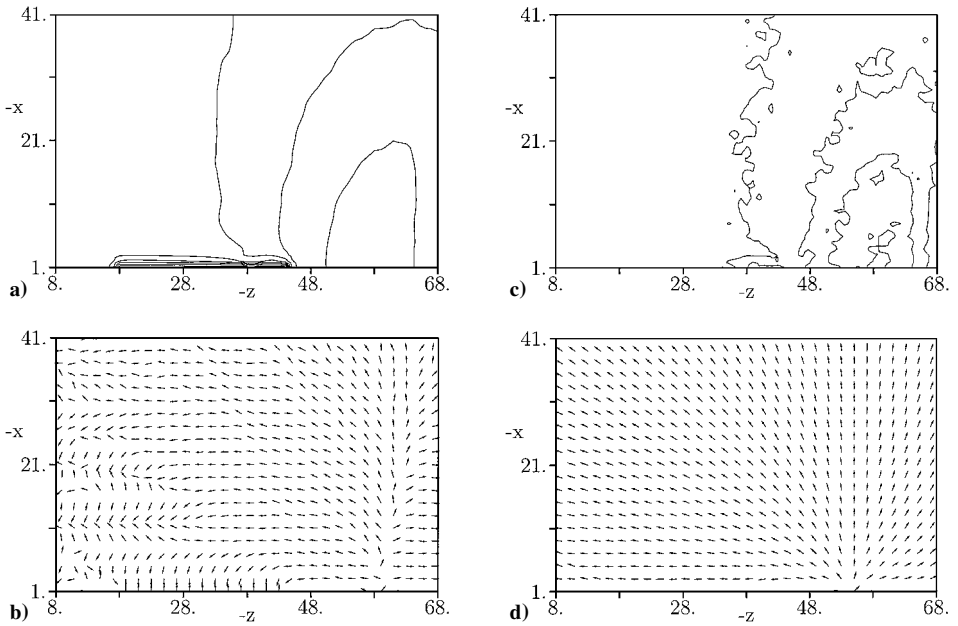

Fig. 7 Simulation results on a zx plane at $y = 30$: a) electric potential (contour levels clockwise from the solar array ($-x = 1$, $-z$ from 18 to 44) toward the right side: $\Phi - \Phi_{sc}$ from 0 to 19 V with an interval of 1 v), b) vector plots for electric field $E/|E|$, c) total ion number density (contour levels clockwise from the solar array toward the right side: $n_i = 5 \times 10^4$, 1.5×10^5, 2.5×10^5, and 3.5×10^5 particles/cm^3), and d) vector plots for charge-exchange ion velocity $J_{cex}/|J_{cex}|$.

ambient potential is not known a priori. However, when a steady state is reached, the potential at the simulation outer boundary represents the ambient potential with respect to the spacecraft.

IDS measurements[3] indicate that the local λ_D^{cex} at the IDS location is on the order of $\mathcal{O}(1)$ cm. In the simulations presented here, the grid resolution is taken to be $d_{\text{cell}} \simeq 6$ cm. Through test simulations we found that using smaller computational cells had little effect on our results. This is because our chosen grid size is already either comparable to or smaller than the local debye length over most of the simulation domain. The total number of grid points used is $43 \times 43 \times 71$.

To obtain meaningful statistics in the backflow region, one needs to use a sufficiently large number of test particles. In the simulations presented here, the total number of test particles in the simulation domain is about 5 million at steady state. The average number of particles per cell ranges from more than 4000 particles per cell in the beam just outside of the thruster exit to a few particles per cell near the left and upper simulation boundary. The entire simulation can be completed in about 5 CPU hours on a Cray SV1-1A supercomputer. Simulations were also performed for different grid resolutions and numbers of test particles to ensure that the simulation results are not affected by simulation parameters.

In the following discussions, the notations x, y, and z are understood to be variables normalized by the cell size d_{cell}. The spacecraft bus is a hexgonal cylinder along the z direction, located at $23 \leq -z \leq 48$. The solar array is a flat plate bounded by $18 \leq -z \leq 44$ and $22 \leq y \leq 44$ on the $-x = 1$ face. The thruster exit center is at $(-x, y, -z) = (1, 1, 49)$.

Figure 3 shows the locations of the spacecraft and the solar array on the $x = -1$ plane along with beam ion density contours calculated from the beam ion model, neutral plume density contours from the neutral plume model, and the contours for the charge-exchange ion production rate calculated from Eq. (5).

In Figs. 4 and 5, we show simulation results on a zy plane cutting through the spacecraft and thruster center at $-x = 1$ and on a zy plane near the spacecraft outer boundary at $-x = 10$, respectively. In Figs. 6 and 7, we show simulation results on a zx plane cutting through the spacecraft and thruster center at $y = 1$ and on a zx plane at $y = 30$, respectively. Figures 4–7 show potential contours, ion density contours, the directions of electric fields $\boldsymbol{E}/|E|$, and the directions of charge-exchange ion current density $\boldsymbol{J}_{\text{cex}}/|J_{\text{cex}}|$.

Because the ion beam is quasi neutral and the beam ion energy E_b is much larger than the potential from the spacecraft, the beam ions are not influenced by the potential field. In contrast to the beam ions, the low energy charge-exchange ions are greatly influenced by the electric field in the plume. Because the electrons are much more mobile than ions, the beam center has a higher potential (Figs. 4a and 4b and Figs. 6a and 6b). As a result, charge-exchange ions produced in the beam flow radially outward from the beam region as shown in Figs. 4c and 4d and Figs. 6c and 6d. The space charge carried by the outflowing charge-exchange ions generates a wing structure near the thruster exit in both the potential contours and ion density contours (the a and c panels in Figs. 4–7).

Once outside the beam region, the charge exchange ions start to expand and interact with the spacecraft. As evident from the c and d panels in Figs. 4–7, an expansion fan structure is generated at the edge of thruster exit surface at $-z = 48$. The velocities of the charge-exchange ions are turned gradually from the radially outward direction in the downstream region to the $+z$ direction near spacecraft surface.

We find that the problem of charge-exchange plasma backflow has the same underlying physics as that of the problem of plasma expansion into a vacuum or plasma wake (see, for example, Refs. 19 and 20 and references therein). Unless the spacecraft is highly charged, the fundamental backflow process is governed by the expansion of a mesothermal plasma. The plasma expansion is similar to the Prandtl–Meyer expansion of a supersonic gas flow over a convex corner (see Ref. 19). The expansion fan is a presheath for the spacecraft, which turns the trajectories of the charge-exchange ions into the upstream direction until they enter into the sheath of spacecraft.

As a result of charge-exchange ion backflow, the spacecraft sees a substantial charge exchange ion density. In Fig. 8, we plot the potential, charge-exchange ion number density, and current density along several x axes in the $y = 1$ plane. The charge-exchange ion density near the spacecraft ranges from 10^6 cm^{-3} at $-z = 50$ (the thruster end) to 10^4 cm^{-3} at $-z = 24$ (the opposite end). Because the charge-exchange plasma density near the spacecraft is at least three orders of magnitude larger than the solar wind plasma density, the plasma environment of DS1 spacecraft is completely dominated by the charge-exchange plasma in the plume.

The thickness of the plasma sheath surrounding a spacecraft is about a few debye lengths of the surrounding plasma. The debye length in the solar wind is typically on the order of 10 m. The debye length in a charge-exchange plasma environment with a density of 10^4 cm^{-3} is on the order of 10 cm. Hence, ion thruster operation will reduce the thickness of the plasma sheath surrounding DS1 from $\mathcal{O}(10)$ to $\mathcal{O}(10^{-1})$ m. As a result, the spacecraft potential will be shielded in the immediate vicinity. The thin sheath is evident in both the potential contour plots and in Fig. 8a.

The simulation also predicts the spacecraft floating potential relative to the ambient. In Fig. 8a, the spacecraft potential is set at $\Phi_{\text{sc}} = 0$ V. The potential at the simulation boundary is floating with respect to the spacecraft. Figure 8a suggests that the spacecraft potential is about -5 V with respect to the plasma at infinity.

In Table 2, we compare simulation results with IDS measurements. In-flight measurement of the charge-exchange ion current

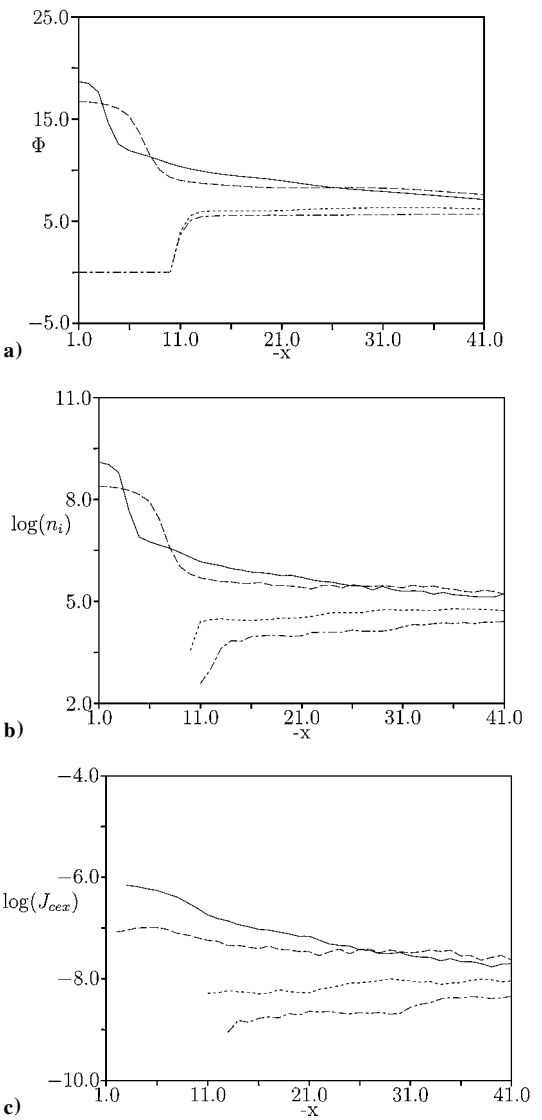

Fig. 8 Physical quantities along several radial directions on the zx plane at $y = 1$: $-z = 50$ (——), $-z = 63$ (- - - -), $-z = 37$ (· · · ·), and $-z = 24$ (–·–): a) potential relative to the spacecraft in volts (spacecraft potential is at 0 V), b) total ion number density in particles per centimeter cubed, and c) charge-exchange ion current density in amperes per centimeters squared (all length variables are normalized by the cell size of 6 cm).

density J_{cex} is obtained from the current collected by IDS-RPA.[3] In-flight measurement of the charge-exchange ion number density n_{cex} is obtained from the current and ion energy measured by IDS-RPA and the local plasma potential measured by IDS-LP1.[3] The IDS-RPA is a four-grid retarding potential analyzer with an individual grid transparency of 0.72. Hence, the minimum ratio of particle flow-through area over sensor surface area is 0.27 (0.72^4). The current registered by IDS-RPA is the current collected at the IDS-RPA surface times a transmission factor, which is less than one but is larger than the flow-through area ratio due to focusing of particles by the electric field in the grids. The actual value of the transmission factor for IDS-RPA is still a subject of ongoing investigation. Because of the uncertainty over this instrument transmission factor, we are only able to determine the lower bound and the upper bound of J_{cex} and n_{cex} for IDS measurements at this moment. Both the lower bound and upper bound values are listed in Table 2. The lower bound values are obtained using the data registered by IDS-RPA and are not corrected for the IDS-RPA transmission factor, that is, the transmission factor is taken to be one. The upper bound values are corrected with a transmission factor that is assumed to equal the minimum flow-through area ratio of 0.27.

The simulation results are taken at a grid point at a location near that of IDS. When they are compared to the IDS results, the computed J_{cex} is a factor of 1.7 of the lower bound and a factor of 0.45 of the upper bound. The computed n_{cex} is a factor of 1.2 of the lower bound and a factor of 0.33 of the upper bound. The major uncertainties in the simulation model include the negligence of any differential charging that may present, the validity of the Boltzmann relationship for the electrons, the assumption that the input value of $\Phi_{p0} - \Phi_{sc}$ is taken to be the measured value of $\Phi_p - \Phi_{scg}$, and the accuracy of the charge-exchange collision cross sections from Rapp and Francis[9] (recent measurements[21] have obtained cross sections larger than those of Ref. 9). Considering all of the simplifications and assumptions involved in our simulation model, the agreement between the simulation and measurement is very remarkable.

V. Conclusions

A fully three-dimensional PIC simulation model of an ion propulsion plasma plume was developed. This model was applied to obtain the induced charge-exchange plasma environment over the entire downstream-to-upstream region surrounding the DS1 spacecraft. When the in-flight ion thruster operating conditions are used as input parameters, the simulation results and measured charge-exchange ion parameters from IDS are in good agreement.

For an interplanetary spacecraft, the physics underlying the charge-exchange plasma spacecraft interaction is the same as that of plasma expansion into a vacuum or plasma wake. Once outside the beam, the charge-exchange ions undergo an expansion process that gradually turns their velocity vector from the radially outward direction to the upstream direction. As a result, the DS1 spacecraft is immersed in a dense charge-exchange plasma environment. Near the spacecraft surface from the thruster end to the opposite end, the charge-exchange plasma density ranges from 10^6 to 10^4 cm^{-3} and the charge-exchange current density ranges from 10^{-7} to 10^{-9} A/cm^{-2} for a typical ion thruster operating condition. Because the charge-exchange plasma density near the spacecraft is at least three orders of magnitude larger than the solar wind plasma density, the plasma environment of the DS1 spacecraft is completely dominated by the charge-exchange plasma in the plume. Because the spacecraft potential is shielded by the thin sheath in the charge-exchange plasma, spacecraft charging potential will not have any significant effect on the backflow of the ionized Mo particles sputtered from the thruster.

Acknowledgments

This research was performed at the Jet Propulsion Laboratory, California Institute of Technology, under a contract with NASA and was supported by NASA New Millennium Deep Space 1 mission and NASA Solar Electric Propulsion Technology Application Readiness Project. Access to the Cray SV1-1A supercomputer used in this study was provided by funding from NASA Offices of Space Science, Mission to Planet Earth, and Aeronautics. We acknowledge many helpful discussions with R. Samanta Roy of the Institute for Defense Analyses; I. Katz of Maxwell Laboratories; D. Young of the University of Michigan; S. P. Gary and J. Nordholt of Los Alamos National Laboratory; B. Goldstein, P. C. Liewer, and J. Polk of the Jet Propulsion Laboratory, California Institute of Technology; and D. Hewett of Lawrence Livermore National Laboratory.

References

[1]Carruth, M. (ed.), "Experimental and Analytical Evaluation of Ion Thruster/Spacecraft Interactions," Jet Propulsion Lab., Publication 80-92, California Inst. of Technology, Pasadena, CA, 1981.

[2]Carruth, M., "A Review of Studies on Ion Thruster Beam and Charge-Exchange Plasmas," AIAA Paper 82-1994, 1982.

[3]Wang, J., Brinza, D., Young, D., Nordholt, J., Polk, J., Henry, M., Goldstein, R., Hanley, J., Lawrence, D., and Shappirio, M., "Deep Space One Investigations of Ion Propulsion Plasma Environment," *Journal of Spacecraft and Rockets*, Vol. 37, No. 5, 2000, pp. 545–555.

[4]Brinza, D., Wang, J., Polk, J., and Henry, M., "Deep Space 1 Measurements of Ion Propulsion Contamination," *Journal of Spacecraft and Rockets*, Vol. 38, No. 3, 2001, pp. 426–432.

[5]Samanta Roy, R., Hastings, D., and Gatsonis, N., "Ion-Thruster Modeling for Backflow Contamination," *Journal of Spacecraft and Rockets*, Vol. 33, No. 4, 1996, pp. 525–534.

[6]Wang, J., Brophy, J., and Brinza, D., "Three-Dimensional Simulations of NSTAR Ion Thruster Plasma Environment," AIAA Paper 96-3202, July 1996.

[7]Katz, I., Davis, V., Wang, J., and Brinza, D., "Electrical Potentials in the NSTAR Charge-Exchange Plume," International Electric Propulsion Conf., IEPC Paper 97-042, Aug. 1997.

[8]VanGilder, D., Font, G., and Boyd, I., "Hybrid Monte Carlo Particle-in-Cell Simulation of an Ion Thruster Plume," *Journal of Propulsion and Power*, Vol. 15, No. 4, 1999, pp. 530–538.

[9]Rapp, D., and Francis, W., "Charge-Exchange Between Gaseous Ions and Atoms," *Journal of Chemical Physics*, Vol. 37, No. 11, 1962, pp. 2631–2645.

[10]Polk, J., Kakuda, R., Anderson, J., Brophy, J., Rawlin, V., Patterson, M., Sovey, J., and Hamley, J., "Validation of the NSTAR Ion Propulsion System on the Deep Space One Mission: Overview and Initial Results," AIAA Paper 99-2274, June 1999.

[11]Boyd, I., VanGilder, D., and Liu, X., "Monte Carlo Simulation of Neutral Xenon Flows in Electric Propulsion Devices," *Journal of Propulsion and Power*, Vol. 14, No. 6, 1998, pp. 1009–1015.

[12]Birdsall, C., and Langdon, A., *Plasma Physics via Computer Simulation*, McGraw–Hill, New York, 1985.

[13]Tajmar, M., and Wang, J., "Three-Dimensional Numerical Simulation of Field-Emission-Electric-Propulsion Neutralization," *Journal of Propulsion and Power*, Vol. 16, No. 3, 2000, pp. 536–544.

[14]Gosling, J., "The Solar Wind," *Encyclopedia of the Solar System*, Academic Press, New York, 1999.

[15]Doss, S., and Miller, K., "Dynamic ADI Methods for Elliptic Equations," *SIAM Journal of Numerical Analysis*, Vol. 16, No. 5, 1979, pp. 837–855.

[16]Hewett, D., Larson, W., and Doss, S., "Solution of Simultaneous Partial Differential Equations Using Dynamic ADI: Solution of the Streamlined Darwin Field Equations," *Journal of Computational Physics*, Vol. 101, 1992 pp. 11–24.

[17]Douglass, J., and Gunn, J., "A General Formulation of Alternating Direction Methods: Part I. Parabolic and Hyperbolic Problems," *Numerische Mathematik*, Vol. 6, 1964, pp. 428–453.

[18]Wang, J., Kondrashov, D., Liewer, P., and Karmesin, S., "Three-Dimensional Deformable-Grid Electromagnetic Particle-in-Cell for Parallel Computers," *Journal of Plasma Physics*, Vol. 61, No. 3, 1999, pp. 367–389.

[19]Wang, J., and Hastings, D., "Ionospheric Plasma Flow over Large High-Voltage Space Platforms. I: Ion-Plasma-Time Scale Interactions of a Plate at Zero Angle of Attack," *Physics of Fluids B*, Vol. 4, No. 6, 1992, pp. 1597–1614.

[20]Wang, J., and Hastings, D., "Ionospheric Plasma Flow over Large High-Voltage Space Platforms. II: The Formation and Structure of Plasma Wake," *Physics of Fluids B*, Vol. 4, No. 6, 1992, pp. 1615–1629.

[21]Pullins, S., Chiu, Y.-H., Levandier, D., and Dressler, R., "Ion Dynamics in Hall Effect and Ion Thrusters: $Xe^+ + Xe$ Symmetric Charge Transfer," AIAA Paper 2000-0603, 2000.

I. D. Boyd
Associate Editor